UNIVERSIDAD TÉCNICA FEDERICO SANTA MARÍA

DEPARTAMENTO DE FÍSICA

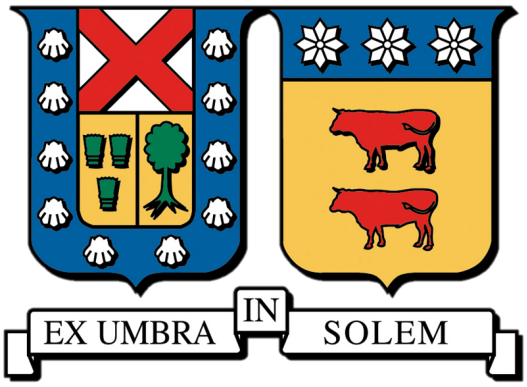

Three new cataclysmic variables from SDSS: are they short period systems?

Ingrith Sharon Achaica Huamani

MEMORIA PARA OPTAR AL TÍTULO DE LA LICENCIATURA EN FÍSICA

PROFESOR: Odette Toloza

April 4, 2024

Abstract

There exist white dwarfs, the remnants of burned-out stars, which accrete material from non-degenerate stars that are helium-rich, known as *AM CVn stars*. These systems are strong sources of gravitational wave radiation and will serve as crucial calibrators for the upcoming LISA mission. Despite their importance, their formation remains unclear. One proposed formation channel suggests they evolve from systems known as cataclysmic variables, in which a white dwarf accretes material from a companion star, which at some point, the external hydrogen layers are depleted, revealing the underlying helium-rich layer.

In this study, I have identified three systems displaying strong helium lines in addition to hydrogen. Therefore, these systems could potentially be transitioning from cataclysmic variables to AM CVn type. A crucial parameter to confirm this transition is the orbital period, as cataclysmic variables reach a minimum period of 70 minutes. Analyzing photometric data from three telescopes: the Zwicky Transient Facility (ZTF) survey, the Transiting Exoplanet Survey Satellite (TESS) satellite mission, and the mexican telescope MEXCAM. I was able to measure a periodicity for one of these systems. Although the period was not robustly identified in one dataset, it was consistently present in all three datasets. I conclude that this periodicity is likely the orbital period, considering the characteristics of the system. Furthermore, this system could represent another potential candidate progenitor of AM CVn through the cataclysmic variable formation channel.

Agradecimientos

I express my gratitude to my thesis advisor, Dr. Odette Toloza, for graciously affording me the opportunity to be under her guidance as her student. Her unwavering support and patience have been instrumental in navigating and shaping the development of my thesis.

Tabla de Contenidos

Acronyms

AMCVN AM Canum Venaticorum.

CE common envelope.

CV cataclysmic variable.

GW gravitational wave.

LMXBs Low-mass X-ray binaries.

SSXB supersoft X-ray binaries.

SyXB Symbiotic X-ray binary.

TESS Transiting Exoplanet Survey Satellite.

WD white dwarf.

WEAVE WHT Enhanced Area Velocity Explorer.

ZTF Zwicky Transient Facility.

Capítulo 1

Introduction

There are white dwarfs that receive mass from a companion enriched with helium, known as AM CVn systems. However, the nature of the companion star remains unclear. Progress in understanding these systems is hindered by their low number, estimated to be around 55. Therefore, it is crucial to discover and characterize these systems to comprehend their formation and evolution. In this work, I aim to measure a key parameter (the orbital period) of three systems, which could potentially be progenitors of AM CVn systems.

1.1 White dwarfs

A white dwarf is a stellar core remnant, primarily composed of electron-degenerate matter, with a mass range less than 8 solar masses. When stars with an initial mass of approximately up to 8 solar masses exhausts their nuclear fuel during the final stages of their evolution, their cores contract under their own gravity. The collapse is halted by electron degeneracy pressure, and the star becomes a white dwarf. If the white dwarf exceeds the Chandrasekhar mass (approximately 1.4 $M_{\odot}$), degeneracy pressure cannot counteract gravitational force, and stellar collapse continues. This can result in a Type Ia supernova, where the entire star is catastrophically destroyed. At birth, a white dwarf emits heat, but over time, it cools down to become a black dwarf. The cooling process, leading to eventual cooling, occurs over timescales that exceed the current age of the universe, as there is no energy generator within the white dwarf, unlike a main sequence star.

In 1910, Henry Norris, Edward Charles, and Willina Fleming discovered the first white dwarf within the triple star system known as 40 Eridani. This system includes a main sequence star orbiting at a certain distance from a closer binary system, composed of a white dwarf and a main sequence red dwarf. It was in 1922 when Willem Luyten officially coined the term "white dwarfs" to refer to these celestial objects. The nearest known white dwarf is Sirius B, located at a distance of 8.6 light years. It is the smaller component of the Sirius binary system, where its companion,

Sirius A, is currently in the red giant phase and is destined to eventually become a white dwarf.

Thanks the pioneer spectroscopic survey, the Sloan Digital Sky survey (SDSS), thousands of white dwarfs have been discovered, and the current count exceeds 30,000 stars. However, this sample has been built with *contaminants* from other scientific objectives, such as QSOs, which introduced several obaservational biases. Presently, white dwarfs are key targets in numerous ongoing spectroscopic surveys, including WEAVE, DESI, 4MOST, and once again in SDSS-V.

1.2 Close white dwarf binaries

It is common to find that white dwarfs in binary systems either as detached stars or interacting systems. The latter cases, the white dwarf accretes matter from a companion, which can be a star, another compact object, or even a planet in some cases. The mass can be transferred due to one of the stars overflows its Roche lobe (largest equipotential) or stellar winds. Next, I will briefly list the types of binary systems that contain white dwarfs.

- cataclysmic variables (CVs): A CV, or Cataclysmic Variable, is a type of binary star system consisting of a white dwarf and a companion star, often a main sequence star. In these systems, the white dwarf accretes material from its companion due to gravitational forces. This material accumulates on the surface of the white dwarf, forming an accretion disk. As the accreted material spirals inward, it releases gravitational potential energy, resulting in the emission of intense radiation across the electromagnetic spectrum, including visible light. This process can lead to periodic variations in brightness and other phenomena, such as nova eruptions and dwarf novae outbursts.

- AM CVn stars: These systems are named after the prototype star, AM Canum Venaticorum. They are white dwarfs accreting from a companion which is rich in helium, which could be another white dwarf or a helium star.

- Low-mass X-ray binaries (LMXBs): Binary systems composed of a neutron star or a black hole. They are called "low-mass" due to the fact that the companion star is typically a red dwarf, a K or M-type star, or even a white dwarf. In these systems are in a very tight orbit, they are called Ultra-compact X-ray binaries (UCXBs). Very few of these systems are known.

- Symbiotic X-ray binary (SyXB): white dwarfs can also have comoanions in which the star has evolved into red giants. In most cases the red giant is typically an M-type stars, but in some cases it can be a yellow giant (G/K-type).

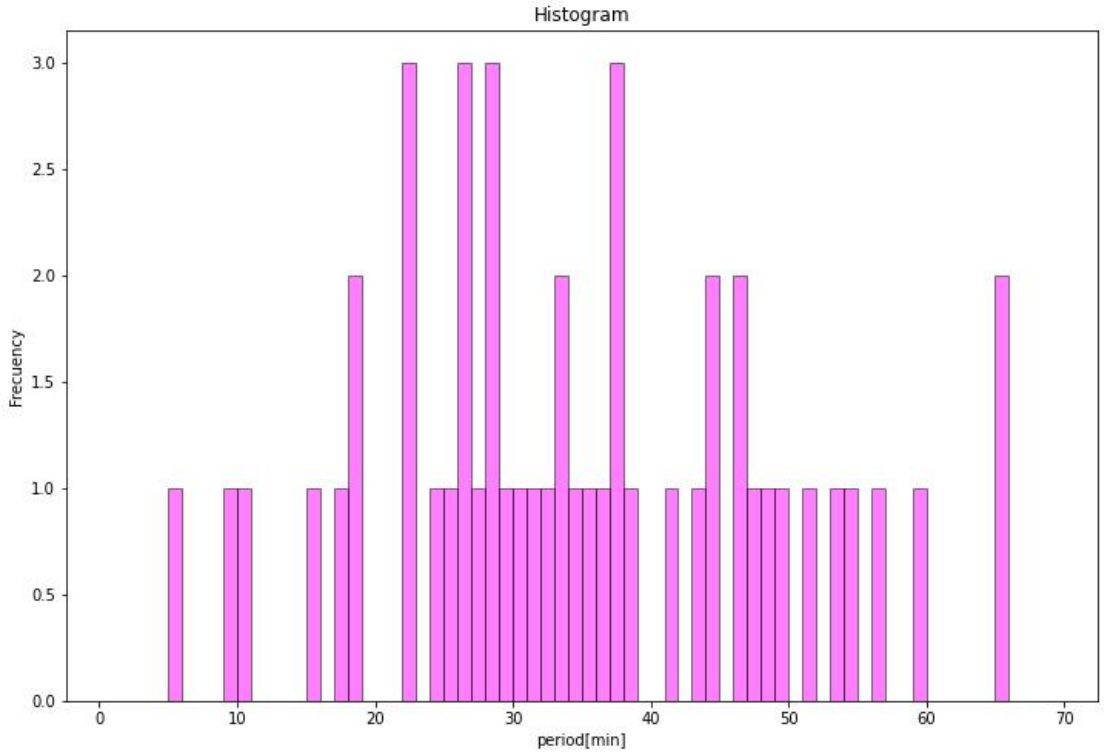

Figura 1.1: Period distribution of AM CVn stars. Sample taken from Ramsay et al. (2018).

- supersoft X-ray binaries (SSXBs): White dwarfs that burn hydrogen stably in close binaries are called super-soft X-ray binaries. The relatively low number of SSXBs and the corresponding low emission of soft X-rays are potentially related to the fact that circumstellar matter may suppress the flow of soft X-rays (Nielsen et al., 2013).

I will emphasize explaining AM CVn stars (alongside cataclysmic variables), as this work involves analyzing spectra that exhibit helium and hydrogen lines.

1.3 AM CVn stars

The AM CVn binaries are of great interest for many aspects of astrophysics. These systems represent the end product of several finely tuned evolutionary pathways (Iben & Tutukov, 1991; Nelemans et al., 2001; Podsiadlowski et al., 2003), and as such are of great interest for binary stellar evolution theory. They are also of particular interest due to their gravitational wave emission, being some of the strongest known sources that would be detected by future low-frequency, space-borne

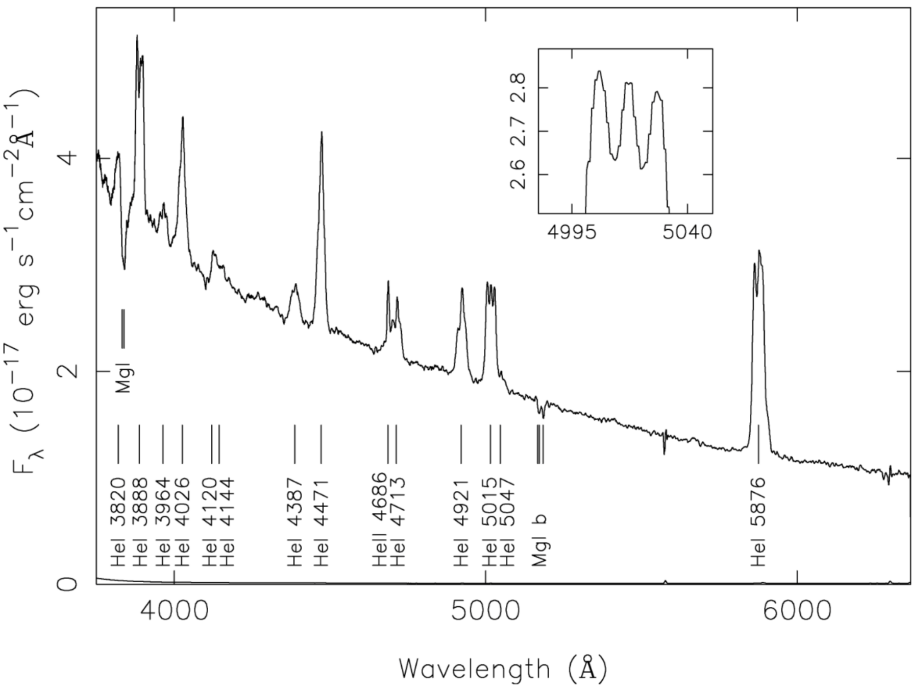

Figura 1.2: Average spectrum of SDSS J1552, an AMCVn star with a long orbitl period of 56.26 min. The fugure show the emission lines of helium and the Mg I absorption triplets. Figure taken from Roelofs et al. (2007)

gravitational wave detectors, the brightest systems acting as calibrators for such an experiment (Stroeer & Vecchio, 2006; Nelemans, 2009).

AM CVn systems can produce thermonuclear supernovae, which are among the most significant explosions in the Universe. The helium that accumulates on a carbon/oxygen white dwarf can undergo unstable thermonuclear flashes when the orbital period falls within the range of 3.5 to 25 minutes. In shorter orbital periods (and higher accretion rates, $\dot{M} > 10^{-7} \approx \text{year}^{-1}$), the flashes are weak. However, as the orbit widens and $\dot{M}$ decreases, the mass required for unstable ignition increases, leading to progressively more violent flashes until a final flash with a helium layer mass of $\approx 0.02 - 0.1$ occurs. The high pressures from these final flashes allow combustion to produce the radioactive elements ^{48}Cr, ^{52}Fe, and ^{56}Ni, which power a faint and rapidly evolving thermonuclear supernova ($M_v = -15$ to -18) over a few days Bildsten et al. (2007).

The first AM CVn system was discovered in 1967 by Smak (1967). Since then, only a few new systems have been discovered, with the total count being just over 50 systems. Most surveys where AM CVn stars have been found have covered only high Galactic latitudes, and it is possible that a substantial fraction reside in the Galactic plane. These systems are challenging to characterize in terms of measuring stellar masses, radii, and orbital periods. However, among the few systems for which orbital periods have been measured, they are found to be in very tight orbits, typically less

than 70 minutes. Figure 1.1 displays a period distribution of AM CVn stars from a sample taken from Ramsay et al. (2018). In contrast, cataclysmic variables have a very well defined minimum period (i.e. 70 mins) they reach, and they bounce back towards longer periods

The principal property of AM CVn in its spectra is the double peaked emission lines. This feature indicated the presence of an acretion disc around the white dwarf. The emission lines in an accretion disc are primarily broadened due to Doppler shifts caused by the motion of the material in the disc falling towards the central object. These lines provide information about the velocity and distribution of the material in the disc. The optical spectra of AM CVn systems exhibit intense emission lines of He I and He II and rarely the Balmer lines (see Figure 1.2). The lines originate from the material in the accretion disk.

The evolution is mainly governed by the loss of angular momentum by gravitational wave radiation (in addition to other mechanisms like magnetic braking which its strength decrease significantly at short periods). This is described by L. D. Landau (1971) for circular orbits. The lost of anugular momentum via gravitationcal radiaton is dictated by the formula

$$\left(\frac{\dot{J}}{J}\right)_{GW} = -\frac{32}{5}\frac{G^3}{c^5}\frac{M_1 M_2 (M_1 + M_2)}{a^4} \tag{1.1}$$

where G is the gravitational constant , c the speed of light, M_1 and M_2 are the masses of the two stellar components, and a is the distance between them.

1.4 Formation and evolution of AMCV stars

Three formation channels have been proposed, all of which involve a common initial phase known as the common envelope phase (Figura 1.3; Belloni & Schreiber 2023). Before explaining the three proposed scenarios, I will describe the initial stages of evolution:

The formation of the AM CVn binary begins with two stars on the main sequence, the primary stage of stellar evolution where stars burn hydrogen in their cores to produce energy. One of the stars evolves off the main sequence. Depending on their initial masses, one of the stars may become a subgiant or a red giant as its core contracts and its atmosphere expands. A common envelope forms around the giant or supergiant, and its outer atmosphere expands beyond its Roche lobe, reaching or enveloping its stellar companion. Although a common envelope event in many situations is triggered by dynamically unstable mass transfer, there are also other mechanisms capable of doing so, such as the Darwin instability (e.g., Hut, 1980), which occurs if the future donor's angular momentum in synchronism exceeds a third of that of the orbit. The Darwin instability corresponds to a tidal instability. It occurs when not enough orbital angular momentum is extracted from the orbit to keep the star synchronized as it evolves. Tidal forces will spin the star

removing the orbital angular momentum, resulting in a binary with a smaller orbital separation and, in turn, even less orbital angular momentum. This implies that the star will need even more orbital angular momentum to stay synchronized with the orbital motion. This leads to an out-of-control process of orbital decay and ultimately to a CE event. Eventually, the common envelope is ejected from the binary system due to orbital energy loss and friction within the envelope. At this point, we have a detach system composed of white dwarf plus a main sequence star: *post common envelope binaries*. From this point the systems can follow different pathways, in which I will describe each of them.

1.4.1 The White Dwarf Channel

Following the initial mass transfer event (the common envelope), the system must lose orbital angular momentum, causing the orbital period to decrease before the secondary star evolves into a red giant, filling its Roche lobe and forming a second common envelope. During this phase, the secondary star evolves into a helium white dwarf. Later, the system loses angular momentum through gravitational wave radiation, causing the carbon/oxygen white dwarf to begin stably accreting mass from the helium white dwarf. This process leads to an ultra-short orbital period, indicating the transformation of the system into an AM CVn binary.

1.4.2 The Helium-Star Channel

The WD/He channel closely resembles the WD/WD channel in terms of their evolution, which is essentially the same. However, the primary difference lies after the final common envelope phase, where the secondary star evolves into a naked helium-burning star instead of a helium white dwarf (HeWD), while the primary star remains a carbon/oxygen white dwarf (C/O WD). Subsequently, angular momentum loss decreases the separation between the two stars, allowing the primary star to accrete helium-dominated material from the (stably) Roche lobe-filling secondary star, resulting in the formation of an AM CVn binary. Similar to the WD/WD channel, the AM CVn binary may have formed either from two consecutive common envelope phases or from stable mass transfer followed by a common envelope phase.

1.4.3 The Hydrogen Star Channel

In contrast to the formation mechanisms discussed earlier, in the CV channel, the second mass transfer phase is dynamically stable, resulting in the formation of a cataclysmic variable (CV). If the donor star in a CV is an unevolved main sequence star, with a hydrogen-dominated core, mass transfer is primarily driven by systemic factors such as gravitational radiation and magnetic

braking, potentially leading to angular momentum loss. The binary follows standard CV evolution, progressing towards shorter periods until the donor star's core becomes partially degenerate, typically at an orbital period of approximately 70 min. At this point, the mass-radius exponent of the donor star changes, and the binary begins to evolve towards longer orbital periods. In cases where the donor star is significantly evolved at the onset of the second mass transfer phase, mass transfer can still be stable, but the binary diverges, resulting in an increase in orbital period as the expansion of the donor star dominates the evolution. If the donor star is neither on the main sequence nor significantly evolved, the CV can evolve into an AM CVn binary. Unlike standard CVs, however, the period bounce phenomenon at approximately 80 minutes does not occur. Instead, the binary progresses towards shorter periods as the donor star becomes increasingly hydrogen-poor. Once the entire hydrogen envelope has been stripped from the donor star, the system transitions into an AM CVn binary.

In general, the properties of donors belonging to AM CVn binaries with orbital periods exceeding ~ 50 minutes are difficult to explain with white dwarf and helium star (section 1.4.2) channels. This is because, regardless of whether the donor is initially a white dwarf with a helium core or a helium star, it will eventually cool and contract during evolution before reaching such long orbital periods. The CV channel has long been considered insignificant for the formation of AM CVn binaries, primarily for two reasons based on theoretical modeling of the CV channel. Firstly, previous calculations (Goliasch & Nelson, 2015; Kalomeni et al., 2016) predicted that AM CVn binaries only form from a very narrow range of parameter space for post-common envelope binaries, implying that AM CVn binaries should be much rarer than they actually are if this channel significantly contributed to their formation. Secondly, earlier evolutionary models suggested that the CV channel always predicts that AM CVn binaries will have detectable amounts of hydrogen in their atmospheres (e.g. Nelemans et al., 2010). Since AM CVn binaries lack hydrogen in their spectra, the classical conclusion was that the CV channel should not significantly contribute to the intrinsic population of AM CVn binaries.

Thanks to the *Gaia* mission, the first statistically significant and unbiased sample of ~ 170000 white dwarf binary candidates have been built. SDSS-V is carrying out a dedicated survey for white dwarfs, single, and in binaries, and we report the analysis of the spectroscopy of 118 cataclysmic variables (CVs) and CV candidates obtained during the first plate observations of SDSS Inight et al. (2023b).

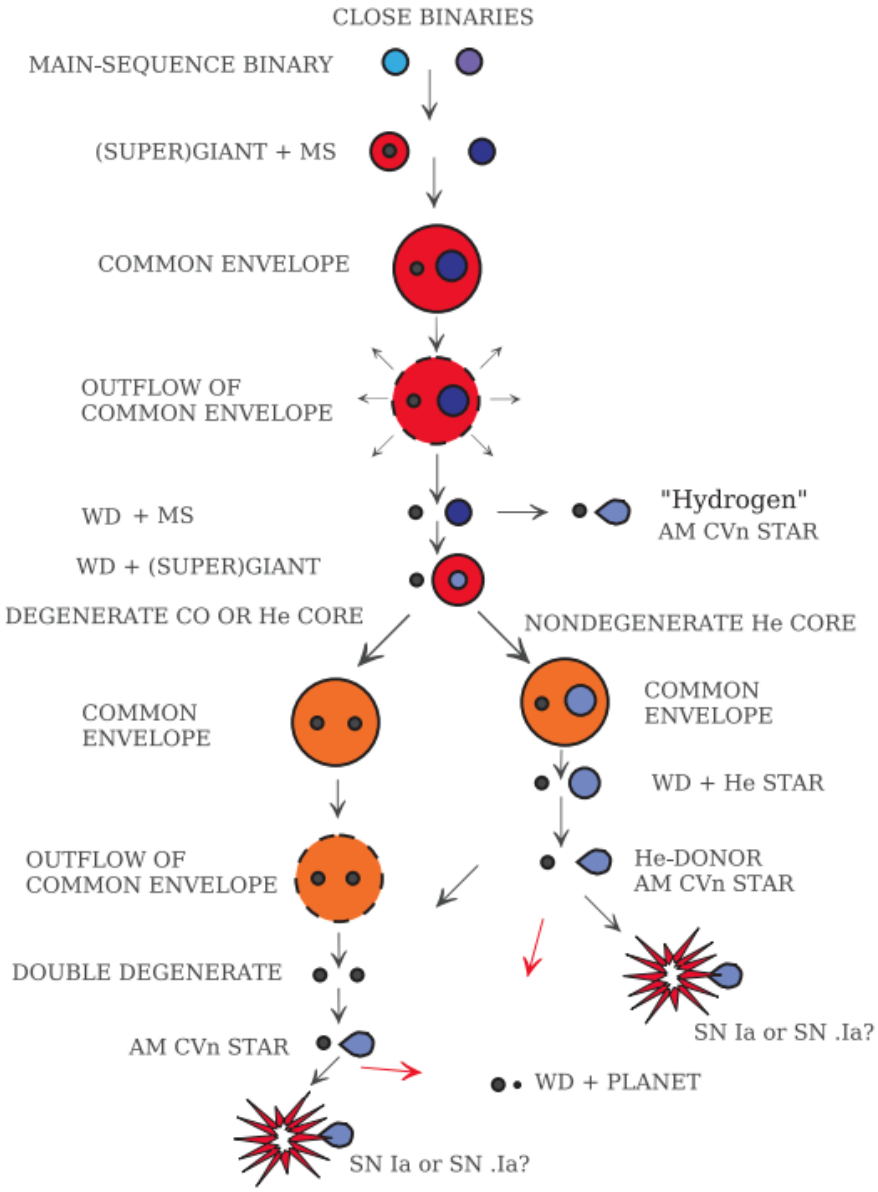

Figura 1.3: Schema showing the evolutionary pathways todars the formation of AM CVn stars from close binaries (prepared by Postnov & Yungelson (2014))

Capítulo 2

The discovery of three short orbital period systems from SDSS

The Sloan Digital Sky Survey (SDSS-V) is an ongoing spectroscopic survey which marks a significant milestone as the inaugural facility to offer multi-epoch optical and infrared spectroscopy spanning the entire celestial sphere. Additionally, it provides seamless integral-field spectroscopic coverage of both the Milky Way and galaxies within the Local Volume. This comprehensive spectroscopic survey upholds the distinguished legacy of the SDSS by delivering pioneering data and collaborative infrastructure. I am member of the sub-survey within the SDSS which aims to obtain spectroscopy of the sample of compact white dwarf binaries. Among the spectra, I classified I identify three spectra which look similar: i.e. the lines do not display the double peak (they are narrow) and the helium lines are stronger than usually seen in normal CVs (for which the hydrogen line mainly dominate). In this chapter I will describe SDSS, the catalogue of the compact white dwarf binaries, and the three objects I identified as short period CVs.

2.1 The fifth generation of the Sloan Digital Sky Survey

The SDSS telescope is a $2.5m$ $f/5$ modified Ritchey-Chrétien wide-field altitude-azimuth telescope located at the Apache Point Observatory (APO), Sunspot, New Mexico (Tutukov & Yungelson, 1996). Ritchey-Chrétien refers to an optical design used in telescopes. It was developed by the American astronomer George Willis Ritchey and the French engineer Henri Chrétien in the first half of the 20th century. The Ritchey-Chrétien design is a variant of the reflecting telescope, which utilizes mirrors to collect and focus light instead of lenses. In a Ritchey-Chrétien telescope, both the primary mirror and the secondary mirror have hyperbolic shapes, which allows for the correction of optical aberrations and improvement of image quality.

The main characteristics of the telescope mentioned in the text are:

- Modified Ritchey-Chrétien $2.5mf/5$ Telescope: It refers to the optical design of the telescope, which utilizes a modified version of the Ritchey-Chrétien design. The telescope has a diameter of 2.5 meters and a focal ratio of $f/5$. This design ensures high image quality and a wide field of view.

- Distortion-Free Wide-Field: The telescope achieves a very wide, distortion-free field of view of up to 3 degrees. This is made possible by incorporating a large secondary mirror and two corrector lenses. The absence of distortions is essential for obtaining accurate and detailed images.

- Photometric/Astrometric Mosaic Camera: The telescope is equipped with a photometric/astrometric mosaic camera. This camera scans the sky along great circles at the sidereal rate. It is mounted at the Cassegrain focus and is used for precise photometric and astrometric measurements.

- Double Fiber-Fed Spectrographs: The telescope features two double fiber-fed spectrographs, which are permanently mounted on the image rotator. The use of fiber feeding ensures stability and prevents flexing during exposures. The telescope can switch between imaging and spectroscopic modes by replacing the imaging camera with a fiber plug plate individually drilled for each field, which feeds the spectrographs.

- Versatile Mounting and Enclosure: The telescope's mounting and enclosure are designed to allow easy access for rapid changes between fiber plug plates and between spectroscopic and imaging modes. This strategy enables imaging to be conducted under pristine observing conditions, such as a photometric sky with image sizes below 1.5 arcseconds full width at half maximum (FWHM), while spectroscopy can be performed under less ideal conditions. All observations are carried out in moonless sky.

2.2 Compact white dwarf binaries in SDSS-V

The cataclysmic variables sample (for observation with SDSS) underwent a two-phase selection process, involving initial identification (to narrow down the number of objects) followed by a visual inspection (for classification). More details are provided in Inight et al. (2023a).

During the SDSS I to IV surveys, which were primarily focused on various astronomical studies, including quasars, there was no explicit targeting of CVs. However, the targets selected for the BOSS and eBOSS surveys included quasars, which occupy a similar parameter space in terms of color to CVs. Over years, a list of CVs was compiled through visual inspection of flux and wavelength calibrated SDSS spectra. This visual process was supplemented by a supervised machine

learning approach. A dataset containing known CVs and non-CVs was used to train a Random Forest (RF) classifier, utilizing features extracted from spectral line equivalent widths and the spectrum's average gradient measured over specific intervals. While there may be CVs that were not identified through this process, due to low signal-to-noise ratio spectroscopy or colors closely resembling single main-sequence stars, we are confident that the majority of CVs were captured in our search.

Classifying cataclysmic variables (CVs) cannot rely solely on one method; rather, it requires the consideration of all available information to establish a consistent classification: Gaia astrometry, and broad-band photometry colors. Composite images were constructed containing all the information, in which multiple reviews of these images were conducted by various individuals, employing pre-selection criteria based on color and filtering according to redshifts determined by the SDSS project. The Figure 2.1 shown an example of the images which were inspected. In the following, I will describe the components in the image one by one.

- The BOSS spectrum in the main panel, with Balmer lines marked in green, Mg II lines in magenta, Ca lines in pink, and Na lines in yellow.
- The Gaia HR diagram in the top right corner, showing the main sequence, giant branch, and white dwarf sequence clearly. The Gaia DR2 (EDR3) position of the target is marked in red (blue).
- A PanSTARRS1 image in the top center, with Gaia objects overlaid, and ultraviolet GALEX detections (orange for NUV, green for FUV, and magenta for both). The dashed circle in the middle represents the size of the BOSS spectrograph fiber, with the target represented by a red circle. Nearby objects are shown as blue circles, with their size proportional to the magnitude difference from the target. Two apparent magnitudes are provided for reference. This image helps assess if the spectrum may be contaminated by light from a nearby source.
- The UV-IR spectral energy distribution is displayed in the top left corner.
- Metadata is collected at the bottom. Warnings are shown in orange/red (discrepancy in magnitude between SDSS spectrum and Gaia target, indication of disconnected fiber).

During my undergraduate studies, I classified over 3000 images. Throughout this process, I noticed three objects that stood out to me (henceforth I will refer to them as Katy, Alin, and David), primarily due to their significant emission of helium lines compared to typical cataclysmic variables (see figure 2.2), which predominantly exhibit hydrogen emission. Consequently, I hypothesize that these objects could be cataclysmic variables evolving towards AM CVn systems,

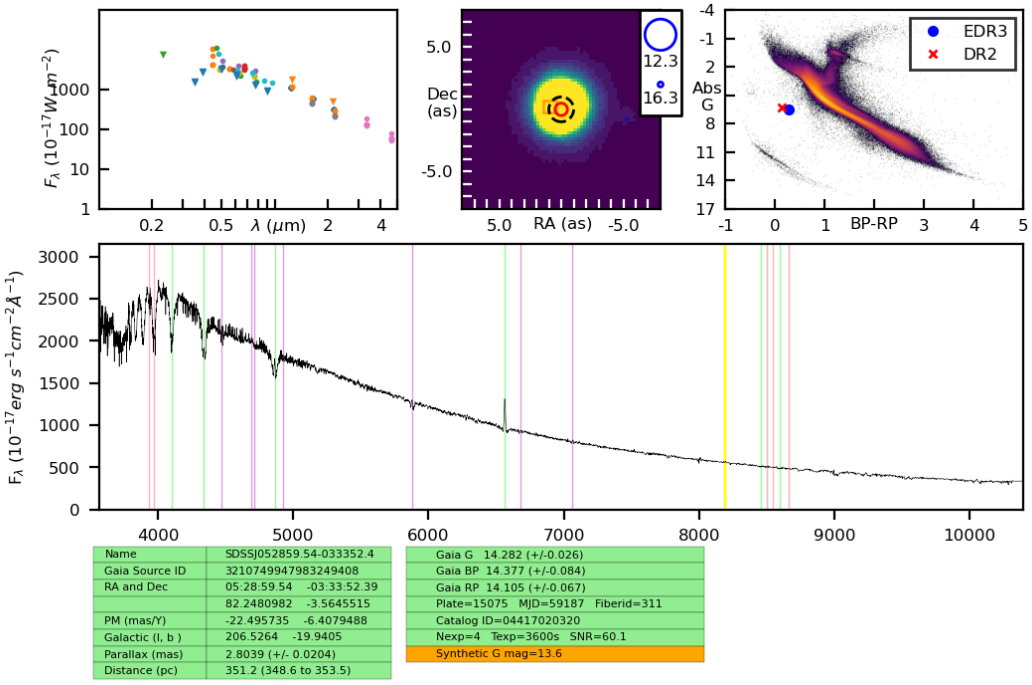

Figura 2.1: PNG from the SDSS wiki, which displays the SDSS spectrum of the cataclysmic variable V1159 Ori (bottom), its position in the HR diagram (top right), an optical image of the Pan-STARSS survey (top middle), and the SED from several surveys (top left). In addition, the figure has at its footnote two tables listing some astrometric and photometric information

specifically through the hydrogen star channel (refer to section 1.4.3). Therefore, a test is to measure its orbital period which is the purpose of this tesina.

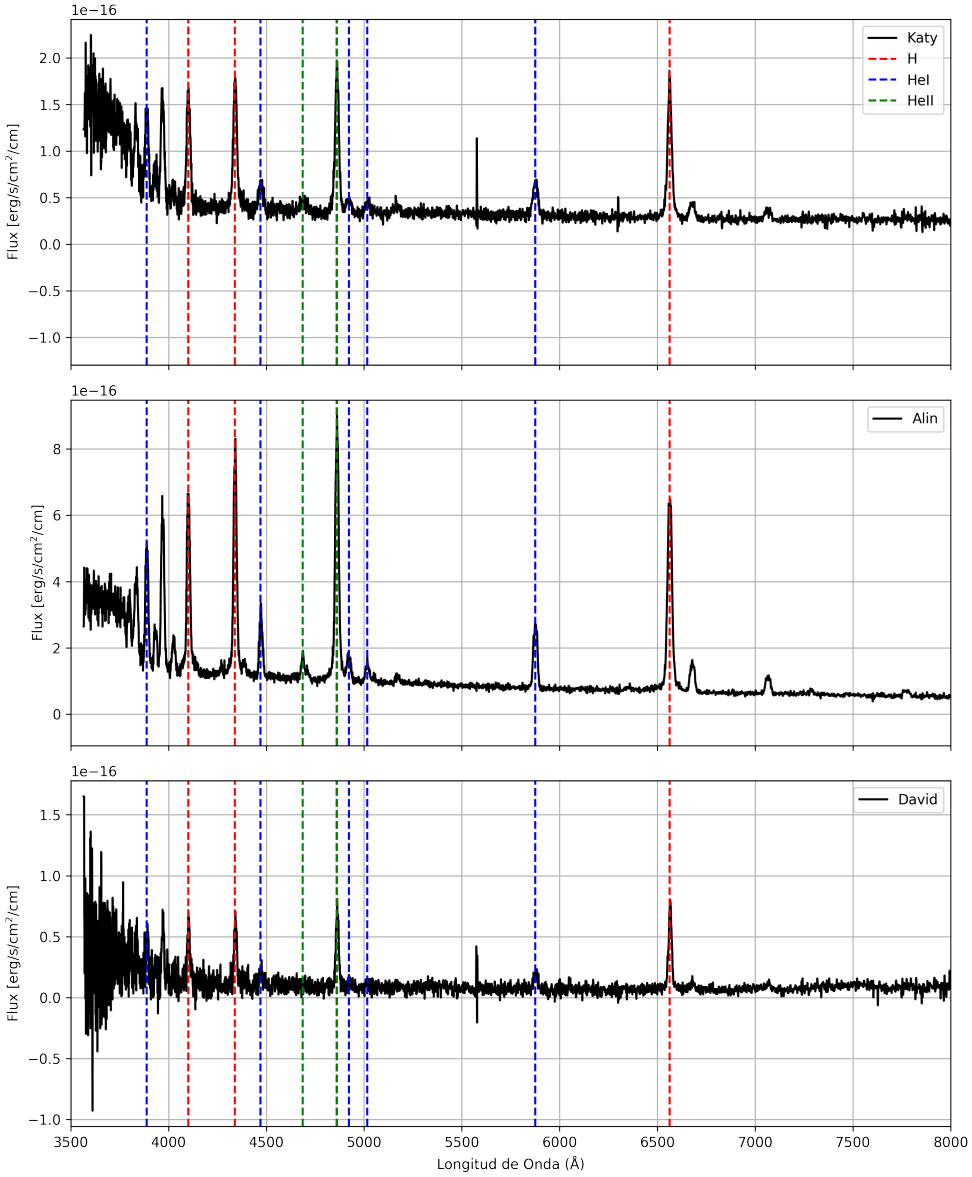

Figura 2.2: The spectra display emission lines of hydrogen and helium. *HeII* at 4686Å(green) is very strong, which is comparable to the emission line of H_α at 6563 Å(red line). The top two spectra in addition display neutral helium (e.g. *HeI* at 5876 Å), while the bottom spectrum spectrum (David) the strength of the line is minimal. The spectroscopic data were extracted from SDSS-V.

Capítulo 3

Observations

These three systems have been observed by two ongoing photometric surveys (the Zwicky Transient Facility and Transiting Exoplanet Survey Satellite), and my team conducted follow-up photometric observations on one of them, yielding indications of periodicity from the photometric data. In this chapter, I will describe the three sources of data for which I performed the analysis.

3.1 Zwicky Transient Facility (ZTF)

The ZTF observation system offers efficient multiband optical imaging with an exceptionally wide field-of-view (see figure 3.1). This system is integrated into the 48-inch Samuel Oschin telescope, known as a Schmidt-type telescope, located at the Palomar Observatory. The central component of this system is a cryogenic CCD mosaic science camera with an astonishing 47 square degrees of field of view and an impressive resolution of 600 megapixels. The use of cryogenic temperatures is crucial in this camera as it allows cooling the CCD sensors to extremely low levels, dramatically reducing electronic and thermal noise. This, in turn, translates to high-quality images, free from interference and with exceptional sharpness (Inight, Gänsicke, Breedt, Israel, Littlefair, Manser, Marsh, Mulvany, Pala & Thorstensen, ZTF). Additionally, this camera is complemented by an innovative aspheric telescope corrector optics, designed to correct optical aberrations. Unlike conventional spherical surfaces, this telescope does not follow the perfect curvature of a sphere, allowing for superior image quality. This system also includes a large-format exposure shutter, characterized by its electronic exposure control capability. This is particularly valuable in large-format telescopes, where electronic shuttering techniques are used to control exposure duration, minimizing any unwanted interference.

Furthermore, a flat field illumination system and a robotic bandpass filter changer have been incorporated for efficient data capture at various wavelengths. A field flattener, an optical element that corrects field curvature, is also used. ZTF builds upon the proven success of the previous PTF

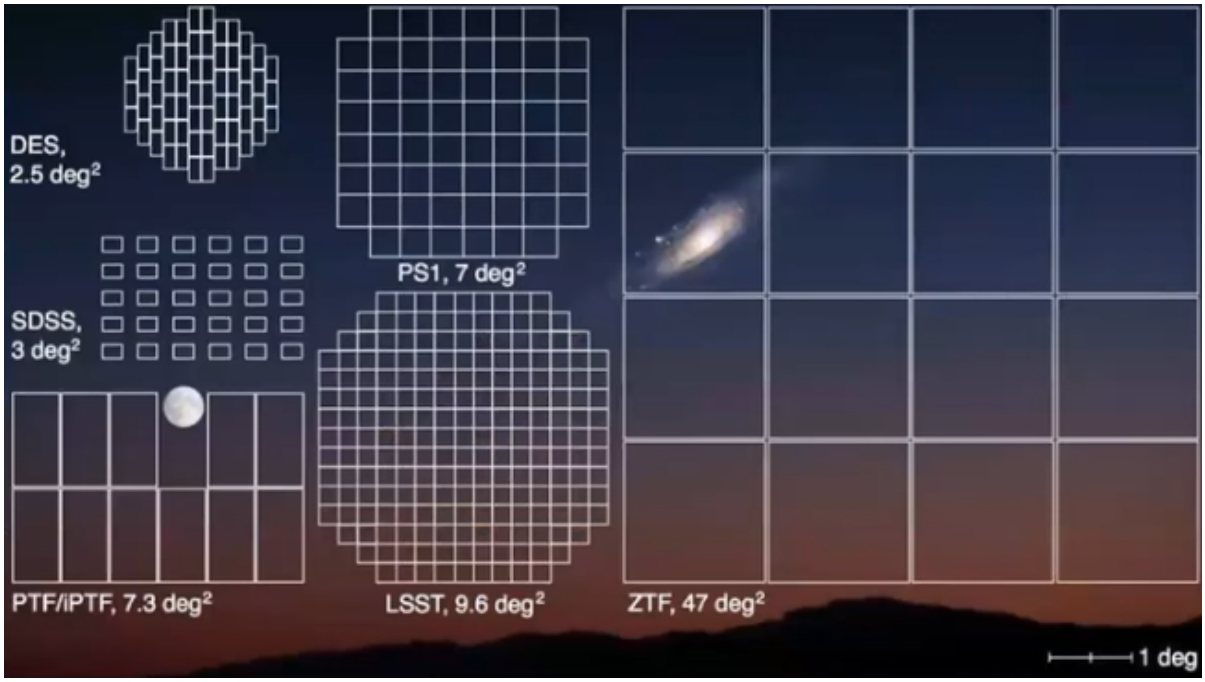

Figura 3.1: Field-of-view of different ongoing and future photometric ground-based surveys, which displays the large sky coverage of ZFT.

survey and has achieved over an order of magnitude increase in survey speed without sacrificing image quality, maintaining an impressive 2.0" FWHM resolution across the entire focal plane. Modern and fast readout electronics add only 10 seconds of overhead per exposure. This telescope uses G (green), R (red), and I (infrared) filters.

I downloaded the ZTF lightcurves for the three systems from the NASA/IPAC infrared science archive[1]. In general, the three objects have been observed by the three filters (i.e. g, r, and i), but we retrieve the data for filter r since it is the one containing the largest number of data points, which is suitable to measure the orbital period of the three systems. In addition, the bandwidth of the r filter is $5,500 - 7,400\,\mathring{A}$, which covers the Balmer α emission line of the systems. The r-band light curves for the three systems are shown in Figure 3.2

3.1.1 Lomb Scargle periodograms

The sampling of the light curve from ZTF is non-uniform, characterized by non-equidistant data points. To address this, an optimized program is employed for computing the discrete Fourier transform. The software `period04` [2] is used to computed the periodograms. It also provide the window function on the dataset, aiding in understanding the temporal sampling nuances of the

[1] https://irsa.ipac.caltech.edu/cgi-bin/Gator/nph-dd
[2] http://period04.net/

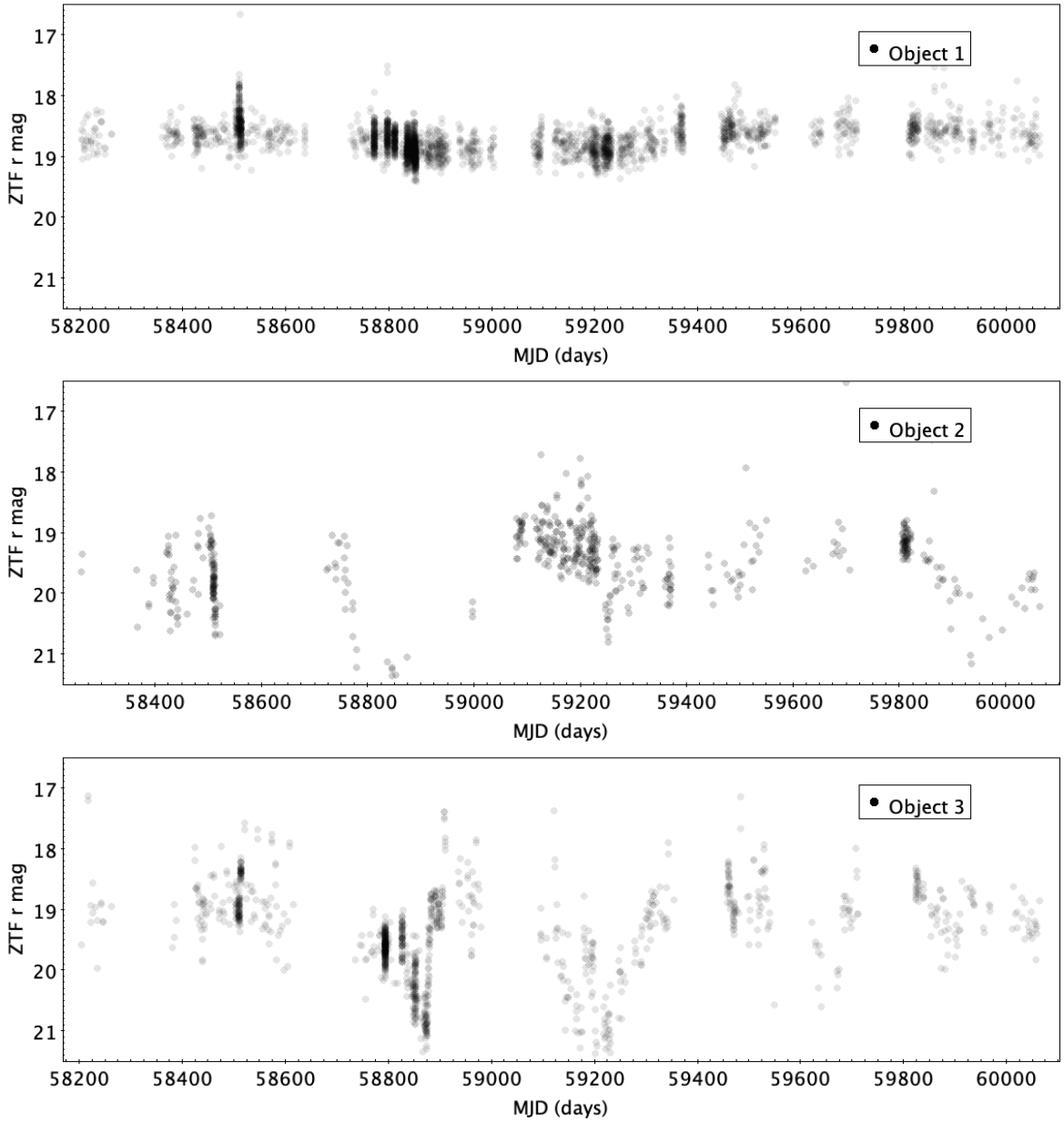

Figura 3.2: ZTF r' band lightcurves for the three systems. The lightcurves show fluctuations in their brightnesses

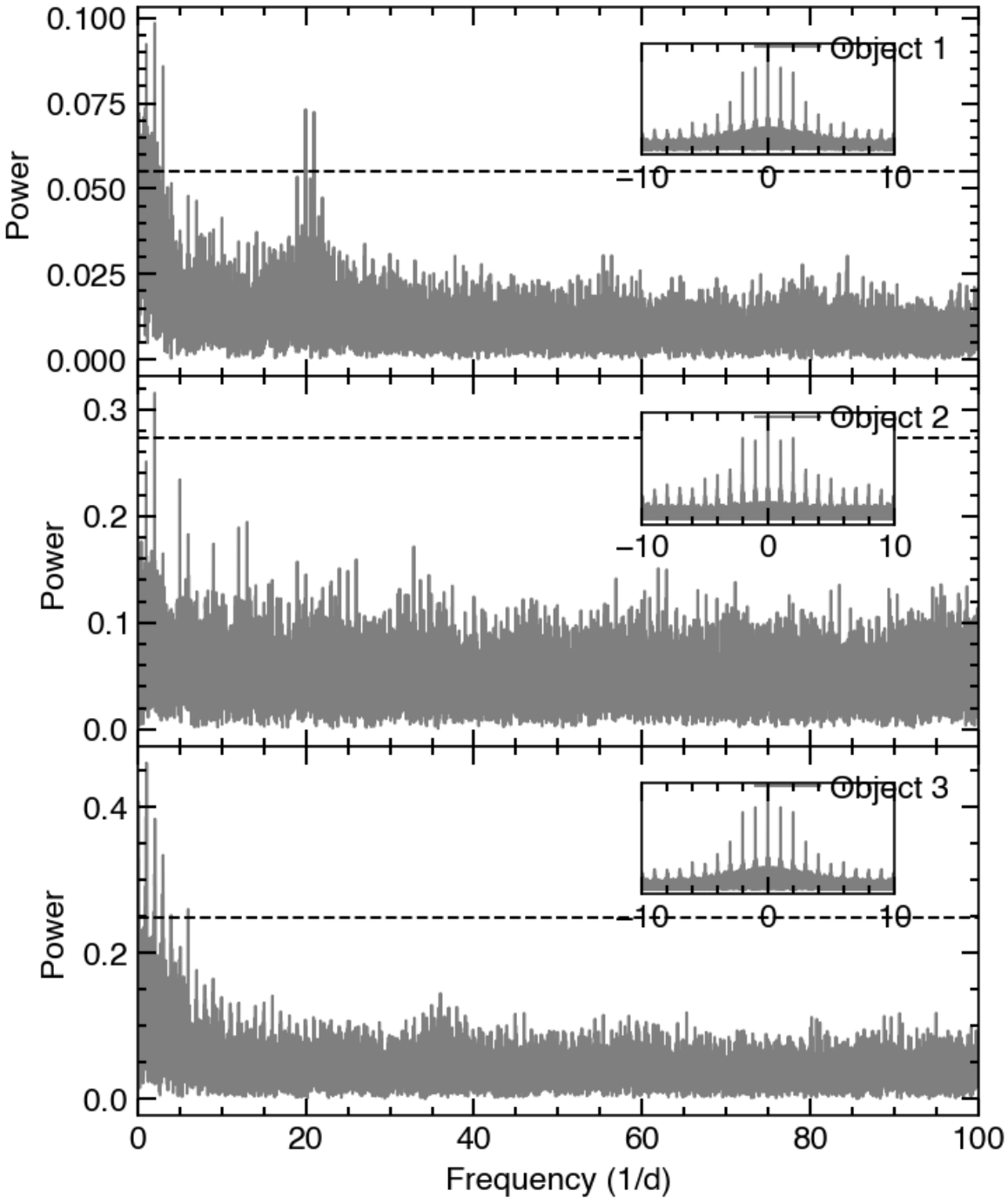

Figura 3.3: Periodograms of the three systems. The horizontal line demarcates the significance level (see text for details). The inset in each panel shows the spectral window. The three systems show peaks at very short frequencies caused by the ZTF temporal sampling. Only the system (object 1) in the top panel, hints at the presence of short frequency at $\simeq 20$ (1/d).

Table 3.1: Frequencies at the maximum power. The peaks in all the power spectra occur at the 2 (1/d), however these peaks are due to aliases introduced by the data sampling of the ZTF observing strategy. Also is shown are the parameters amplitude and phases of the best sinusoidal fit to the lightcurve, which a visual inspection does not describe any periodic trend

ID	Name	F_{Nyquist}	noise	step rate	freq1 +/- error	amplitude +/- error	phase +/- error
obj 1	Katy	1019	0.066	3.26	2.01028 ±0.00003	0.094±0.006	0.66±0.01
obj 2	Alin	211	0.092	0.626	2	0.24± 0.05	0.77±0.02
obj 3	David	1000	0.215	1.26	1.04±0.01	0.4±0.1	0.38±0.09

light curves, including the identification of any aliases present. The periodograms together with the spectral windows are displayed in Figure 3.3. The algorithm implemented in PERIOD04 calculates the Nyquist frequency (shown in Table 3.1) using the average time gap between neighboring points while ignoring large gaps.

Subsequently, the power spectrum is calculated to discern periodicities within the light curve data. In general, the three periodograms display prominent peaks at very short frequencies. Consequently, a significance level is determined using the distribution of the data of the power. This significance level is shown with a horizontal dashed line in Figure 3.3, which I defined at 10 times the standard deviation above the mean of the power distribution. The highest peaks of the periodograms correspond to very short frequencies, which the values are listed in Table 3.1. None of these frequencies describe the behavior of the lightcurves, and these peaks are a consequence of the data sampling process. To simplify, I assigned different names to the objects to aid in easier recall (Table 3.1).

Interestingly, the system named Katy exhibits a potential periodicity at frequency around 20 (1/day), which transforms into a period of $P = 70$ min This ambiguous period is investigated further utilising additional photometry in the following sections (section 3.2 and section 3.3).

3.2 The Transiting Exoplanet Survey Satellite (*TESS*)

TESS mission is a space-based telescope designed to search for exoplanets orbiting the brightest stars in our vicinity. It was launched by NASA in April 2018 and has been conducting its mission since then. The survey strategy focuses on observing nearby and relatively bright objects, divided into 26 sectors which coves the entire celestial globe. Each sector covers an area of the sky measuring 24 degrees by 96 degrees, which allows *TESS* to monitor a significant portion of the celestial sphere, enabling *TESS* to observe more than 200,000 stars simultaneously, searching for the characteristic brightness changes associated with exoplanet transits (see Figure 3.4 for more technical specifications).

The three systems studied in this work have been observed by *TESS*. Cuts of the *TESS* images

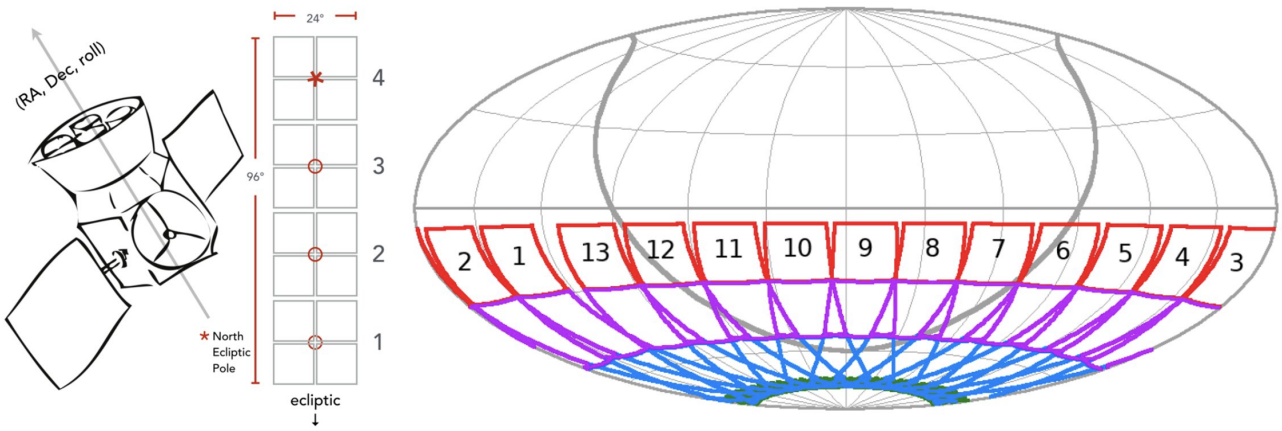

Figura 3.4: Transiting Exoplanet Survey Satellite (*TESS*) has a field-of-view of 24ºx96º which is oriented along a line of ecliptic longitude with the instrument boresight generally pointing at ±54º ecliptic latitude, which centers Camera 4 on an ecliptic pole: camera 1 is red, camera 2 is magenta, camera 3 is blue, camera 4 is green (close to the pole). Observations during Year 1 comprised Sectors 1-13. For each of these sectors, the instrument boresight was pointed at an ecliptic declination of -54º

.

are shown in Figure 3.5, illustrating the positions of the targets with black crosses. As evident from the images, the targets appear very faint, posing challenges for their detection. Moreover, Katy and David are accompanied by very bright sources nearby. Table 3.2 presents a log of all observations conducted by *TESS*.

The *TESS* team provides the lightcurves to the community in data releases of the sectors. The lightcurves produced by TESS data processing pipeline, which is currently being developed by the Science Processing Operations Center (SPOC). At the time of writipng up this document, only Katy has light curves available generated by the SPOC pipeline. This pipeline processes raw pixels to extract photometry centered on the targets' positions for each star, based on astrometry. It also identifies and eliminates systematic errors. The SPOC team focuses on exoplanetary science, particularly the detection of eclipses in the *TESS* light curve, so their pipeline is optimized for such searches. Consequently, developers provide two flux arrays: (1) raw data with no additional correction and (2) corrected data, which is normalized and has trends removed. I retrieve the only SPOC lightcurve with no additional correction that is available to the date using the python package LIGHTKURVE. The lightcurve from sector 60 taken during 2022 is shown in the left panel in Figure 3.6. Each datapoint in the lightcurve is extracted from the concatenation of 60 *TESS* images (i.e. every 120 seconds). The data cover about one month presenting few gaps of data. The periodogram is presented in the right panel in Figure 3.6, which similarly to the ZTF analysis (previous section 3.1), it also presents low frequency peaks, in addition shows a peak around 20

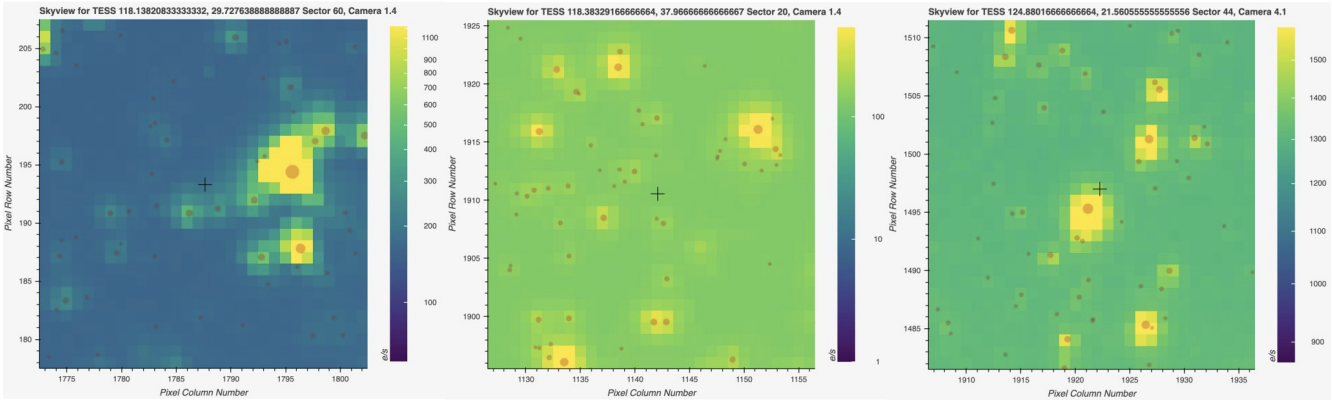

Figura 3.5: TESS FFI cuts of 30 × 30 pixels square (i.e. field-of-view of 110 armin square) corresponding to the first frame of the time series array. The black cross demarcates the position of our object of interest, which from left to right they corresponds to the systems Katy, Alin, and David. The light red dots overplotted show the positions of the sources that fall within the field-of-view which have been identified by Gaia DR3 (the size of the circle is proportional to the brightness of the source).

Table 3.2: Log of the *TESS* observations. Sector 46 is not processed since the target fell very close to the edge making difficult to compute the brightness. Object marked with an asterisk (*) the system falls too close to the edge of the CCD

Target name	Sector	Date	Exp. time (s)	cycle	camera	CCD
Katy	20	2019-Dec-24 to 2020-Jan-21	1426	20	1	4
Katy	20	2019-Dec-24 to 2020-Jan-21	1426	2	1	4
Katy	44	2021-Oct-12 to 2021-Nov-06	475	4	4	1
Katy	45	2021-Nov-06 to 2021-Dec-02	475	4	2	3
Katy	46	2021-Dec-02 to 2021-Dec-30	475	4	1	3
Katy*	47	2021-Dec-30 to 2022-Jan-28	475	4	1	4
Katy	60	2022-Dec-23 to 2023-Jan-18	158	5	1	4
Alin	20	2019-12-25 to 2020-02-14	1426	2	1	4
Alin	47	2021-12-31 to 2022-02-11	475	4	1	3
Alin	60	2022-12-23 to 2023-02-07	158	5	1	4
David	44	2021-Oct-12 to 2021-Nov-06	475	4	4	1
David	45	2021-Nov-06 to 2021-Dec-02	475	4	2	2
David	46	2021-Dec-02 to 2021-Dec-30	475	4	1	2

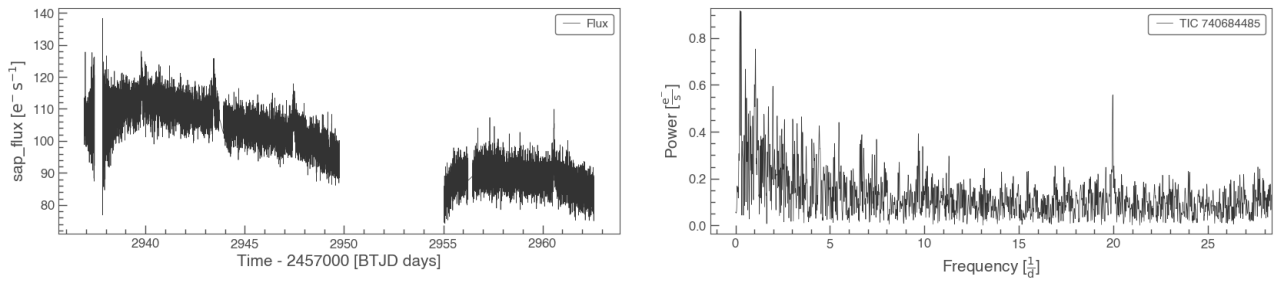

Figura 3.6: *Left:lightcurve of Katy. Right: periodogram of Katy*

(1/d). For this dataset, I did not investigate the significance given that the peak is evident just by a quick visual inspection.

However, there are some considerations regarding this finding. Firstly, Katy is very faint, and *TESS* is most effective for bright M-type stars ($V < 16$ mag). Secondly, *TESS* has a large pixel size (i.e., 21 arcsec), which in crowded regions may lead to flux contamination from nearby sources. As illustrated in the left panel of Figure 3.5, the source is not fully resolved and is accompanied by a bright nearby source, potentially contaminating the light curve provided by SPOC. A deeper statistical analysis on the data is required in order to check if the periodicity is real and that comes from Katy, thus as a future work this period can be analised by `tess_localize`. This tools involves determining the position of a variable source in the sky and identifying the most probable *Gaia* source based on *TESS* pixel data and observed frequency variations (Higgins & Bell, 2023).

3.3 84cm telescope in Mexico (MEXCAM)

The targets were observed with the 0.84m telescope situated in Mexico in OAN San Pedro Martir (MEXCAM). Our collaborator from UNAM university on México got awarded 5 nights to obtain photometric data. Unfortunately, 1.5 nights were lost due to bad weather conditions, and thus only two out of the three targets were able to be observed (Katy and Alin). The acquisiton of the calibration files failed, in particular the flats. Thus, the analysis presented here are on images that have not been corrected from flatfielding. However, the images are steady, i.e no large shifts are detected of the source on the position of the target on the CCD.

I calculated the power spectrum using PERIOD04 for both objects shown in Figure 3.7 for Katy. The light curve displays a smooth decline, which I speculate that the system could might have undergone an outburst and it is returning back to quiescence. Similar, to the ZTF data (see section 3.1) I detect a mild peak around 20 (cycles/day) which turns clearer during the second night. For this dataset, I set a significance threshold as 3 sigma above the mean of the power spectrum (red dashed line in Figure 3.7).

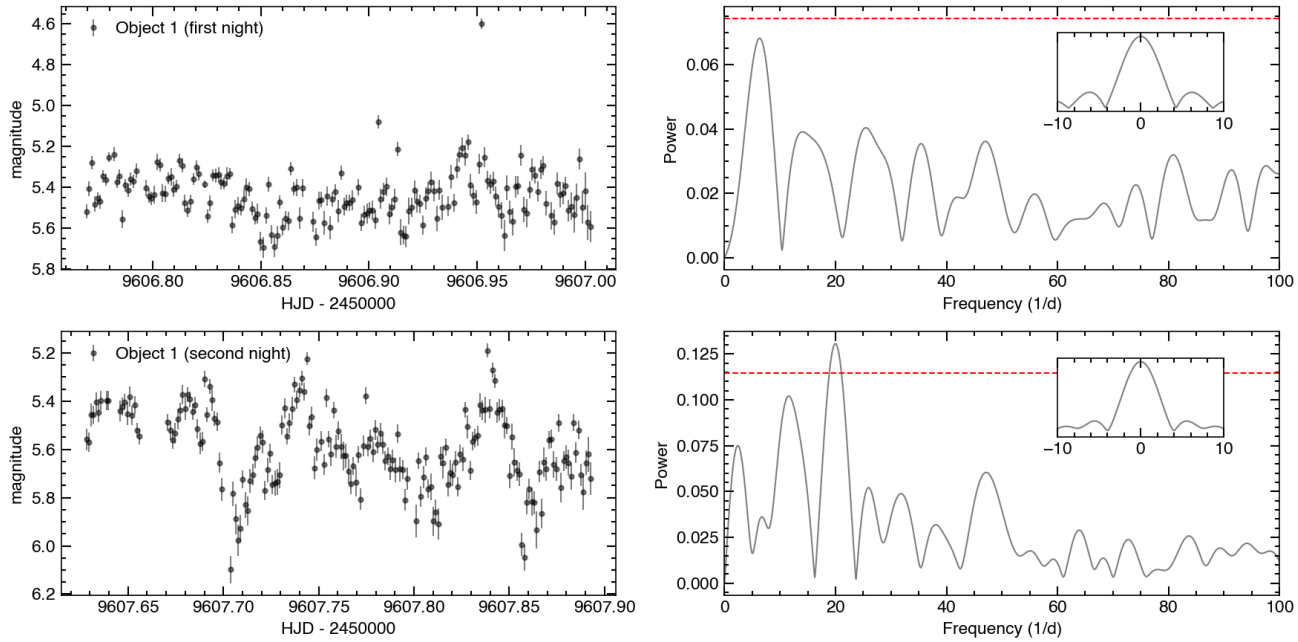

Figura 3.7: The light curve of Katy was observed for two nights, as shown on the left. The respective periodograms are observed on the right. During the second night, a period of 20 cycles per day was obtained, equivalent to 70 minutes.

Capítulo 4

Results and conclusions

Table 4.1 provides a summary of the periods identified in the three systems. Only in one of them (Katy) was the period consistently measured in all three datasets analyzed; however, its ambiguity raises questions about its reliability, despite being detected in multiple data sources. The source of this periodicity could potentially be the orbital period of the system. Alternatively, other mechanisms may be at play, such as the rotation of the white dwarf, which could create a heated spot due to the accretion of material channeled by magnetism. This could also explain the detection of helium II emission in the spectrum. However, since the spectra show double-peaked emission lines indicative of gas moving in Keplerian orbits (i.e., a disc), under these circumstances, the systems could also be a magnetic system, known as intermediate polar. The reason we can rule out this possibility is that typically a second periodicity, known as the beat period, would be detected. This beat period arises from the changing accretion from the south magnetic pole to the north magnetic pole and vice versa.

Table 4.1: Orbital periods

name	ZTF	TESS	84cm
Katy	$\simeq$70 min	$\simeq$70 min	$\simeq$ 70 min
Alin	None	-	-
David	None	-	-

As cataclysmic variables accrete material from hydrogen-rich stars, the companion star gradually erodes until fusion ceases, transforming into a quasi-degenerate sub-stellar object. At this point, cataclysmic variables do not reduce their orbital period but begin to expand. This occurs at a very precise orbital period of 70 minutes, which is the value measured for Katy. Therefore, although Katy does not fall within the regime of AM CVn systems, it could be a candidate progenitor of a system evolving towards AM CVn. Thus, Katy represents a crucial object for constraining evolutionary models along this pathway.

Referencias

Belloni D., Schreiber M. R., 2023, Astron. Astrophys., 678, A34

Bildsten L., Shen K. J., Weinberg N. N., Nelemans G., 2007, The Astrophysical Journal, 662, L95

Goliasch J., Nelson L., 2015, The Astrophysical Journal, 809, 80

Higgins M. E., Bell K. J., 2023, AJ, 165, 141

Iben Icko J., Tutukov A. V., 1991, Astrophys. J., 370, 615

Inight K., et al., 2023a, Mon. Not. R. Astron. Soc., 524, 4867

Inight K., et al., 2023b, Mon. Not. R. Astron. Soc., 525, 3597

Kalomeni B., Nelson L., Rappaport S., Molnar M., Quintin J., Yakut K., 2016, Astrophys. J., 833, 83

L. D. Landau E. L., 1971, Publ. Astron. Soc. Pacif., volume 2, 193

Nelemans G., 2009, Classical and Quantum Gravity, 26, 094030

Nelemans G., Portegies Zwart S. F., Verbunt F., Yungelson L. R., 2001, Astron. Astrophys., 368, 939

Nelemans G., Yungelson L. R., van der Sluys M. V., Tout C. A., 2010, Mon. Not. R. Astron. Soc., 401, 1347

Podsiadlowski P., Han Z., Rappaport S., 2003, Mon. Not. R. Astron. Soc., 340, 1214

Postnov K. A., Yungelson L. R., 2014, Living Reviews in Relativity, 17, 3

Ramsay G., et al., 2018, Astron. Astrophys., 620, A141

Roelofs G. H. A., Groot P. J., Steeghs D., Marsh T. R., Nelemans G., 2007, Mon. Not. R. Astron. Soc., 382, 1643

Smak J., 1967, Acta Astron., 17, 255

Stroeer A., Vecchio A., 2006, Classical and Quantum Gravity, 23, S809

Tutukov A., Yungelson L., 1996, Monthly Notices of the Royal Astronomical Society, 280, 1035

Zwicky Transient Facility (ZTF), https://www.ztf.caltech.edu/